



Exoskeleton dissolution with mechanoreceptor damage in larval Dungeness crab related to severity of present-day ocean acidification vertical gradients

Nina Bednaršek ^{a,*}, Richard A. Feely ^b, Marcus W. Beck ^c, Simone R. Alin ^b, Samantha A. Siedlecki ^d, Piero Calosi ^e, Emily L. Norton ^f, Casey Saenger ^f, Jasna Štrus ^g, Dana Greeley ^b, Nikolay P. Nezlin ^a, Miranda Roethler ^a, John I. Spicer ^h

^a Southern California Coastal Water Research Project, Costa Mesa, CA 92626, USA

^b NOAA Pacific Marine Environmental Laboratory, 7600 Sand Point Way NE, Seattle, WA 98115, USA

^c Tampa Bay Estuary Program, 263 13th Ave S, St. Petersburg, FL, 33701, USA

^d Department of Marine Sciences, University of Connecticut, Groton, CT 06340, USA

^e Département de Biologie, Chimie et Géographie, Université du Québec à Rimouski, 300 Allée des Ursulines, Rimouski, QC G5L 3A1, Canada

^f Joint Institute for the Study of the Atmosphere and Ocean, University of Washington, Seattle, WA 98195, USA

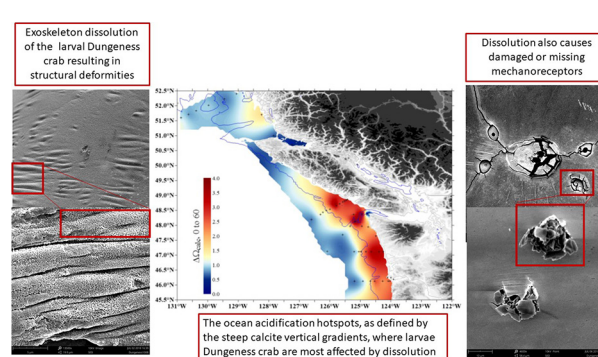
^g Department of Biology, Biotechnical Faculty, University of Ljubljana, Ljubljana, 1000, Slovenia

^h University of Plymouth, School of Biological and Marine Sciences, Plymouth PL4 8AA, UK

HIGHLIGHTS

- Coastal habitats with the steepest ocean acidification gradients are most detrimental for larval Dungeness crabs.
- Severe carapace dissolution was observed in larval Dungeness crabs along the US west coast.
- Mechanoreceptors with important sensory and behavioral functions were destabilized.
- Dissolution is negatively related to the growth, demonstrating energetic trade-offs.
- 10% dissolution increase over the last two decades estimated due to atmospheric CO₂.

GRAPHICAL ABSTRACT



ARTICLE INFO

Article history:

Received 8 November 2019

Received in revised form 4 January 2020

Accepted 7 January 2020

Available online xxx

Editor: Henner Hollert

Keywords:

Dungeness crab

Larval sensitivity

ABSTRACT

Ocean acidification (OA) along the US West Coast is intensifying faster than observed in the global ocean. This is particularly true in nearshore regions (<200 m) that experience a lower buffering capacity while at the same time providing important habitats for ecologically and economically significant species. While the literature on the effects of OA from laboratory experiments is voluminous, there is little understanding of present-day OA *in-situ* effects on marine life. Dungeness crab (*Metacarcinus magister*) is perennially one of the most valuable commercial and recreational fisheries. We focused on establishing OA-related vulnerability of larval crustacean based on mineralogical and elemental carapace to external and internal carapace dissolution by using a combination of different methods ranging from scanning electron microscopy, energy dispersive X-ray spectroscopy, elemental mapping and X-ray diffraction. By integrating carapace features with the chemical observations and biogeochemical model hindcast, we identify the occurrence of external carapace dissolution related to the steepest Ω calcite

* Corresponding author.

E-mail address: ninab@sccwrp.org (N. Bednaršek).

Global climate change
 Ocean acidification
 Exoskeleton structure
 Dissolution
 Mechanoreceptor damage

gradients ($\Delta\Omega_{\text{cal},60}$) in the water column. Dissolution features are observed across the carapace, pereopods (legs), and around the calcified areas surrounding neuritic canals of mechanoreceptors. The carapace dissolution is the most extensive in the coastal habitats under prolonged (1-month) long exposure, as demonstrated by the use of the model hindcast. Such dissolution has a potential to destabilize mechanoreceptors with important sensory and behavioral functions, a pathway of sensitivity to OA. Carapace dissolution is negatively related to crab larval width, demonstrating a basis for energetic trade-offs. Using a retrospective prediction from a regression models, we estimate an 8.3% increase in external carapace dissolution over the last two decades and identified a set of affected OA-related sublethal pathways to inform future risk assessment studies of Dungeness crabs.

© 2020 Elsevier B.V. All rights reserved.

1. Introduction

Since the pre-industrial era, anthropogenic CO_2 uptake along the US West Coast have resulted in rapid intensification OA rate on a global scale (Chavez et al., 2017; Feely et al., 2016), resulting in lower carbonate conditions compared to the pre-industrial times. This is because of the low regional buffering capacity, which contributes to low pH and carbonate mineral saturation states for both aragonite (Ω_{ara}) and calcite (Ω_{cal}) (Feely et al., 2018). These changes in carbonate chemistry have resulted in substantially reduced habitat suitability for marine calcifiers (Bednaršek et al., 2014; Somero et al., 2015). These findings are supported by the field and synthesis work along the North American Pacific demonstrating that calcifying invertebrates will be the ones most impacted by progressive OA (Bednaršek et al., 2017; Busch and McElhany, 2016). Apart from evidence of OA impacts on pteropods and other calcifiers caused by the low Ω_{ara} conditions in upwelling systems (Bednaršek et al., 2014, 2017) and around CO_2 vent seeps and sites (Manno et al., 2019; Tunnicliffe et al., 2009), there is limited understanding of present-day OA effects on marine life *in situ*. That is especially relevant for the crustaceans since they were considered less sensitive to OA parameters (like pCO_2 or pH) after studies demonstrated their capacity to abate initial hypercapnia and to buffer extracellular acid-base disturbances (Melzner et al., 2009; Pane and Barry, 2007) with limited or no change in aerobic metabolism (Paganini et al., 2014). However, restoring internal pH to sustain physiological and biogeochemical processes (Somero, 1986), typically requires activation of buffering, which is energetically expensive process (Cameron, 1985; Michaelidis et al., 2005). Recent experimental findings have demonstrated increased sensitivity to OA-related stressors in crustaceans, especially in the early life stages that can be regarded as a potential bottleneck for the population level responses (Schiffner et al., 2014; Small et al., 2015). Regardless of the habitats that different species inhabit, the studies investigating OA effect on larval stages reported lower growth and decreased survival of blue crab (Giltz and Taylor, 2017), delayed metamorphosis in the stone crab (Gravinese et al., 2018), changes in exoskeleton composition (Page et al., 2016) and decreased metabolisms in Tanner crabs (Long et al., 2016) and increased energetic costs in the porcelain crab (Carter et al., 2013), while the pre-larval of the Dungeness crab showed reduced survival and slower progression through the development (Miller et al., 2016). With annual revenues up to \$220 million (Hodgson et al., 2018; Pacific States Marine Fisheries Commission, 2019), the Dungeness crab (*Metacarcinus magister*) is one of the most valuable and recreational fisheries in the US coastal waters. Terminal stage of pelagic Dungeness crab larvae (megalopae) undergoes long distance transport along the north Pacific coast of North America before settling in suitable benthic settlement site (Shanks, 1995; Sinclair, 1988). Given their diel vertical migration extends down to 60 m depth (Hobbs et al., 1992), megalopae encounter steep vertical pH, Ω_{cal} gradients in coastal habitats; however, the duration and magnitude of their exposure to these conditions remains largely unknown despite the exposure history notably impacting organismal responses (*sensu* Bednaršek et al. (2017)).

To start addressing potential OA vulnerability of the pelagic Dungeness larvae *in situ*, their spatial distribution must be paired with

in situ exposure history (as defined in Bednaršek et al., 2017), understanding of their physiological susceptibility and their structural and mineralogical features. In regards to the later, surprisingly little is known about these features that can predispose an individual to extensive exoskeleton dissolution if the conditions in the external environment are conducive for it. In addition, for detecting environmental clues, the decapod exoskeleton contains elongated hair-like structures called setae, which are important chemo- and mechanoreceptors involved in sensory and behavioral responses. While the lipoproteic epicuticle-covered exoskeleton consists of two cuticular mineral carbonate layers (Chen et al., 2008) (*i.e.*, the outer exocuticle and the inner endocuticle) in the Dungeness crab adults such structure or its composition is completely unknown for the larvae.

This interdisciplinary study integrates physical, geochemical, biological, and modelling components across the individual and population-level parameters. Identification of the carapace crystalline mineralogical and elemental composition provided an understanding behind the extensive exoskeleton dissolution and mechanoreceptor damage. The latter was linked with the chemical observations made along the North American West Coast to identify the drivers and OA hotspots of *in situ* megalopae vulnerability. The biogeochemical model hindcast was used to determine the impact of *in situ* exposure history in the coastal habitats.

2. Materials and methods

2.1. Carbonate chemistry, sampling and analyses

For the purpose of this study, the NOAA West Coast Ocean Acidification (WCOA) cruise in May–June 2016 sampled conductivity, temperature, depth, and oxygen. Data on the conductivity, temperature, and pressure of seawater (CTD) were collected along cross-shelf transects, accompanied by biological stations with vertical sections of temperature (T), salinity, nutrients, oxygen, chlorophyll-a (chl-a), dissolved inorganic carbon (DIC), total alkalinity (TA), spectrophotometric pH (measured at 25 °C and corrected to *in situ* temperatures, and expressed on the total pH scale, subsequently expressed pH_T). pCO_2 and calcite saturation state (Ω_{cal}) were calculated using CO2SYS as described by Feely et al. (2016) and Bednaršek et al. (2012). Larvae were collected using Neuston and Bongo nets with a mesh size of 333 μm , which were deployed in an oblique manner at 10 stations during the night in the upper surface waters, an area that encompasses the nocturnal vertical habitat of larval Dungeness crabs of the upper 60 m (Hobbs et al., 1992; Morgan, 1989), with the following environmental parameters along the vertical habitat (Table S1). The duration of tows was 15–20 min. Megalopae were identified and then stored in 100% non-denatured ethanol, and also flash-frozen at -80 °C for later comparison of two different preservation methods.

2.2. Using SEM methods to detect and evaluate carapace dissolution

Megalopae carapaces were investigated using a combination of different methods: 1) scanning electron microscopy (SEM; Hitachi Phenom, USA) to determine potential structural changes on the cuticular

surface; 2) energy dispersive X-ray spectroscopy (EDXS at the University of Washington) for mineralogical composition; 3) elemental mapping; and X-ray diffraction (University of Washington and Max Planck Institute) for elemental content across mostly lipoproteic carapace (Fig. S1, Fig. 1). Here, we define exoskeleton as the cuticle covering the dorsal part of the carapace of the larval crab, and five pereopods, with chelae. The carapace epicuticle, which otherwise overlies the crystalline layer and makes dissolution observations impossible, was removed from each megalopa prior to analysis. This was accomplished using sodium hypochlorite, which efficiently removes the epicuticle but does not damage the crystalline layers underneath, even at high concentrations (Bednaršek et al., 2012). On the samples with no hypochlorite treatment, the epicuticle covered the crystalline layer so no investigation of dissolution was possible. Therefore, we tested different concentrations and duration of hypochlorite treatment on the individuals from the same station to ensure that we fully removed the epicuticle, without triggering dissolution of the calcite crystalline layers beneath it. The combination of 1 and 3% sodium hypochlorite with 15, 30, and 120 min treatments only partially removed the epicuticle, while 6% hypochlorite treatments for 4 and 6 h were effective in epicuticle removal, without inducing additional dissolution at the longer duration.

To determine the treatment does not induce any damage, we have tested the individuals from the same stations with different combination of treatments. We assumed the similarity of exposure history of individuals within the same stations (see modelling section). The results of no difference in dissolution under the different combination of concentration/duration of treatment combination was a confirmation that the treatment did not induce any additional damage, and thus did not confound our field observations.

We determined 6% hypochlorite for 3–4 h to be an efficient and effective treatment, similar to the treatment previously described for the removal of the periostracum in pteropods (Bednaršek et al., 2012). After soaking in sodium hypochlorite, samples were rinsed several times in Millipore water to remove any organic matter remaining on the surface of the exoskeleton. It is important to note that when examining the presence of setae within the neuritic canals, we did not use any treatment in order to avoid any methodological artifacts. When examining the internal area of the cuticle, we avoided examining the proximity of the gills given that dissolution could be impacted by the processes around. To quantify the dissolution of internal carapace cuticle, the pereopods and soft tissue of larvae were gently removed from the rest of the body and washed in Millipore water to remove any remaining tissue or organics before treatment with sodium hypochlorite. Each of the five

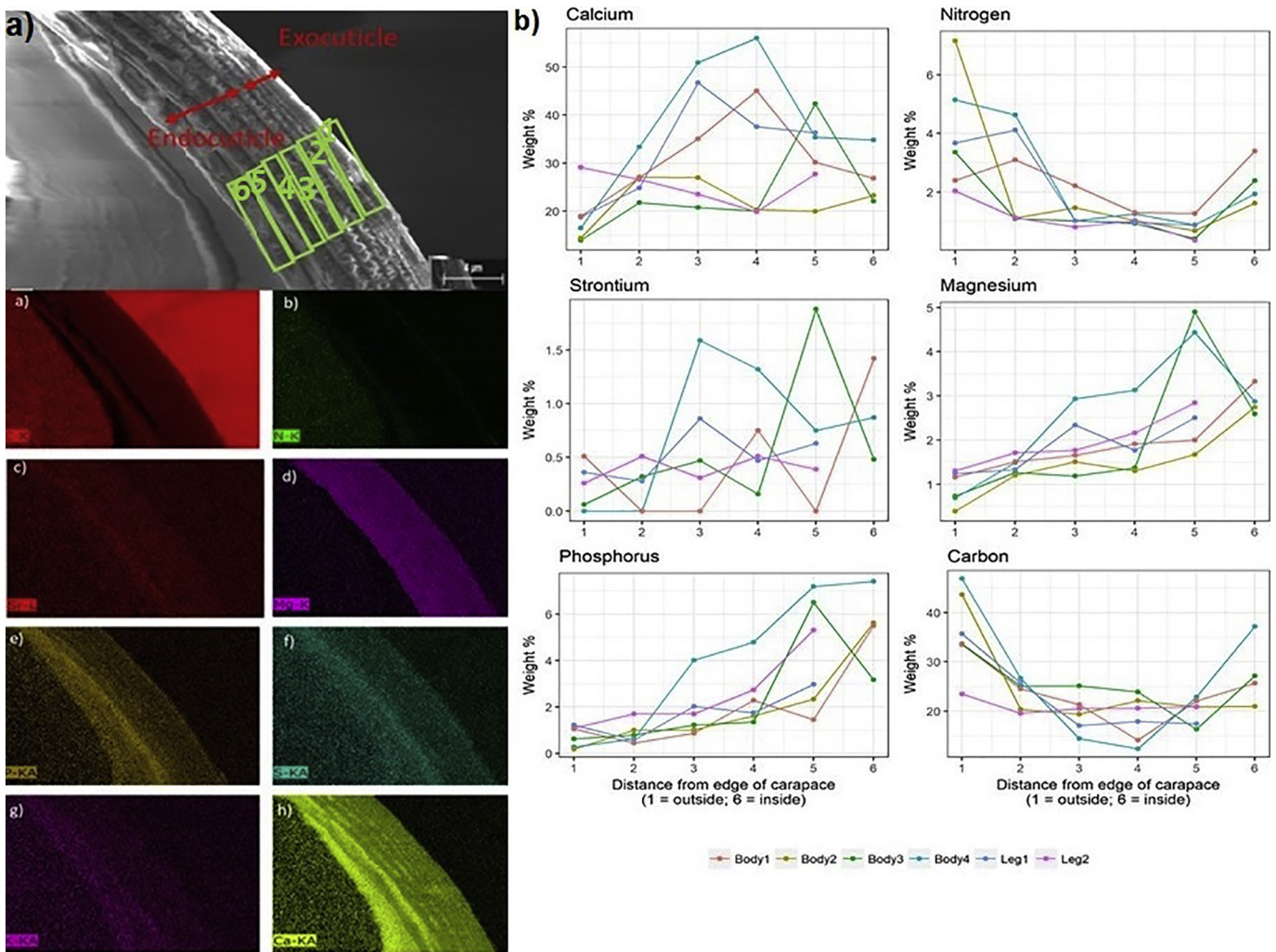


Fig. 1. The cross sections of the Dungeness crab megalopae. Left panel (a): cross section of carapace (with increasing numbers describing the transition from the thinner exo- (1) to thicker endo-cuticle (6). Right panel (b): distribution of various elements (C-carbon-a; N-nitrogen-b; Sr²⁺- strontium-c; Mg²⁺- magnesium-d; P-phosphor-e; S-sulphur-f; K-potassium-g. Ca²⁺- calcium-h). The more intense colors depict higher elemental concentration. Spectrum and % content of selected elements in either carapace or pereopod exoskeleton (a). The numbers in (a) coincide with the numbers in (b) that indicate the position within the carapace.

pereopod cuticle was examined across the proximal and distal ends, with particular focus on chelae (Fig. S2). SEM was used to evaluate the extent and severity of dissolution. We focused on three distinct features: ridging structures, dissolution around setae, and exposed calcite crystals (Fig. S2, S3).

For estimating the various body parameter change (in mm) of larvae across various vertical OA gradients, we have measured carapace length (CL), total length from rostrum to telson (TL), length from rostrum to dorsal carapace spine (R-DCS), and carapace width (CW). The CW is the most commonly used parameter by various US federal agencies along the US West Coast to regulate crab management catch efforts (Davis et al., 2017). Here, we assume that all the larvae were released at the same time to allow for body parameter comparisons across different stations. Using the methodology to characterize the megalopae stages by González-Gordillo et al. (2004), we determined that all megalopae were in the intermolt stage, except for those from Station 115, which were transitioning into the premolt stage. We excluded the results of the internal dissolution observations from this station in case promoting process changed any features on the internal side that could bias accurate dissolution assessment.

2.3. Semi-quantitative dissolution assessment

Altogether, we analyzed 50 individuals from 10 environmental stations across OA-related vertical gradients of varying strength. We used 3–5 individuals per station to determine dissolution extent of the external side of carapace cuticle, as well as the cuticle of the pereopods. We used an additional 2–3 individuals per station to analyze the internal side of the cuticle. Approximately 10–20 SEM images were produced per individual on the external and internal sides, with the images being manually examined to detect any signs of dissolution. For crystal exposure characterization, the same categorization of dissolution conditions as previously described in pteropods was used (Bednaršek et al., 2012). We identified three major features of exoskeleton dissolution and developed a categorization scheme for all three features, showing them in their intact forms (Stage 0, Fig. S2) and progressively altered forms (Stage 1 and 2; Fig. S1; Table S2). These features differentiated damaged surfaces from the intact surfaces (Table S2). The cuticular surface of the carapace and the pereopods under high Ω_{cal} *in situ* conditions had a smooth, sleek appearance (Fig. S2; Stage 0). At greater magnification, individual calcite crystals were visible in these areas (Fig. S2). Signs of dissolution tended to be more prevalent and more severe on the surface immediately surrounding setae pores. Consequently, areas around the setae were considered separately from the rest of the exoskeleton. From these observations, a semi-quantitative scoring metric was developed based on previous work on pteropods and used to score the remainder of the samples. For each sample, the three separate features (presence and depth of ridge structures, exposure of individual calcite crystals, and the prevalence of dissolution features around setae pores) were each assigned a score. The features were scored on a scale of 0 to 1 based on the severity of dissolution: intact exoskeleton with no dissolution received a score of 0; moderate dissolution received a score of 0.5; and substantial dissolution of all examined features was scored 1 (Figs. S1–S3). Since the crab exoskeleton of the carapace and pereopod differ in their chemical composition, these three areas were assigned separate scores. Because of the surface analyses required separately for the external and internal dissolution, both types of analyses could not be conducted on the same individual. All three features displayed similar trends, so the scores were averaged to unitless 'relative dissolution', describing internal and external dissolution. Observation of setae presence/absence was included in the exoskeleton observation under SEM on intact specimen before any preparation treatments were conducted to eliminate the possibility of preparation steps affecting setae presence or outrooting them from the carapace.

2.4. Mineralogical analyses

The mineralogy of selected megalopae was characterized using X-ray diffraction (D8 Discover 2D; University of Washington, Seattle). Prior to analysis, carapaces from five megalopae at each site were coarsely crushed and treated for 10 min using a dilute (3%) sodium hypochlorite solution to minimize interference from organic matter but without compromising mineralized structures. Samples were dried completely and then ground to a fine homogenous powder representing the aggregate of the five individuals from each location. Resulting diffractograms were compared to a catalog of mineral-specific patterns to constrain the primary mineralogy of each sample.

2.5. Elemental analyses

We used energy-dispersive X-ray spectroscopy (EDXS) to estimate elemental composition of the carapace and pereopod cross-sections ($N = 7$) from samples across different natural OA vertical gradients over spatial scales. For elemental analyses, we have not removed the epicuticle from the samples. These gradients analyses were conducted at Max Planck Institute for Marine Microbiology in Bremen, Germany. Prior to analyses, we dehydrated samples using 100% ethanol and dried them in a critical point dryer. We prepared the sections by fracturing different carapace regions which was followed by the EDXS investigations (Fig. 1).

2.6. Statistical analyses

Biological measurements from Dungeness megalopae collected at 10 stations along the North American Pacific Coast (Fig. 2) were paired with synoptic environmental data from CTD profiles. Environmental data were summarized as depth-integrated averages from the surface to the maximum depth of each CTD profile to characterize the exposure conditions in the upper water column. In addition, $\Delta\Omega_{\text{cal},60}$ was estimated as the difference from the observed measurement at each depth bin with that of the surface. This measurement characterized the relative Ω_{cal} gradients with increasing depth and accounted for differences in the relative magnitudes of Ω_{cal} between stations. Chlorophyll-*a* observations were highly skewed and so were log-transformed prior to analysis.

Biological responses included dissolution, body parameter, and abundance with various environmental vertical gradients to identify significant associations using generalized linear models. For comparison of the biological data to environmental conditions, each depth bin for the depth-integrated values was evaluated to identify at which depth associations between biological response and selected environmental variables were strongest. In addition, carapace dissolution was compared to body parameters to characterize potential linkage between the physiological parameters, growth, and population-level effects (abundance). Comparisons of biological measures to each other were also accomplished with generalized linear models.

Gaussian distributions were assumed for all response variable models, excluding presence/absence, which was modeled using a binomial logistic response curve. Models and individual parameters were considered significant at $\alpha = 0.05$. All models had $N = 10$ except presence/absence models with $N = 24$, which included additional stations where tows were conducted but no crabs were found. Finally, all variables were evaluated together to identify pairwise associations using Pearson correlation analysis and redundancy analysis (RDA) to characterize how the biological response measures were jointly explained by the environmental variables. For the latter analysis, all input data were standardized to range from 0 to 1 to account for differences in scale between variables. The *vegan* package for the R statistical programming language was used for standardization and RDA (Oksanen et al., 2019; R Core Team, 2019).

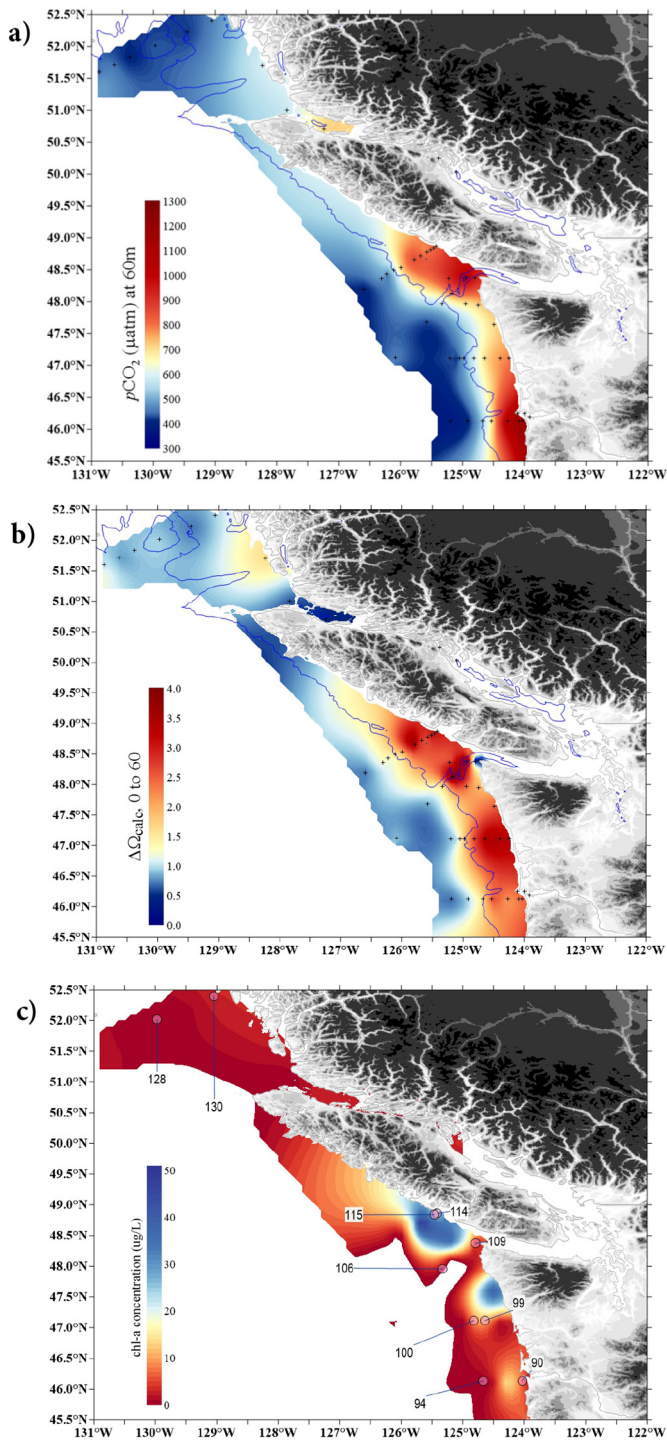


Fig. 2. Interpolated $p\text{CO}_{2,60}$ (a), $\Delta\Omega_{\text{calc},60}$ (b) and chlorophyll (c) conditions in the onshore and offshore habitats along the US West Coast in June 2016. $p\text{CO}_2$ reflects the conditions at 60 m depth and $\Delta\Omega_{\text{calc},60}$ indicates the difference between the surface and 60 m depth. c) Chlorophyll distribution and concentration (chl-a; $\mu\text{g/L}$) demonstrate an order of magnitude difference between the regional nearshore and offshore region. The numbers indicate the stations at which the crabs were collected.

For selected predictors, additional models were developed to evaluate the additive effects of two predictors on dissolution. Backward model selection was used to identify the most parsimonious model by sequentially dropping individual predictors and comparing Akaike Information Criterion values (AIC) (Akaike, 1973; Fox and Weisberg, 2011). This allowed us to determine if there was any additional power in combining predictors to explain dissolution, or consequently, if

dissolution could be sufficiently explained using only one predictor. For example, the ability of both Ω_{calc} and chlorophyll to explain dissolution were evaluated to better understand the relative effects of both.

2.7. J-SCOPE model outputs of the larval exposure history prior to sampling

The Joint Institute for the Study of the Atmosphere and Ocean (JISAO)'s Seasonal Coastal Ocean Prediction of the Ecosystem (J-SCOPE, <http://www.nanoos.org/products/j-scope/>) features dynamical downscaling of regional ocean conditions in Washington and Oregon waters (Siedlecki et al., 2016). Model performance and predictability examined for sea surface temperature (SST), bottom temperature, bottom O_2 , pH, and Ω_{ara} through model hindcast, reforecast, and forecast comparisons with observations, showing significant measurable skill on seasonal timescales (Kaplan et al., 2016; Siedlecki et al., 2016; Norton et al., *in revision*). Megalopae exposure histories were simulated by releasing 100 representative particles, with vertical migration behavior over 60 m inserted into the predicted circulation field at each of the *in situ* sampling locations and times, and then tracking them backward in time for 30 d following methods described for pteropods in Bednaršek et al., 2017, and for megalopae in Norton et al., *in revision*. The vertical migration behavior was simulated using the LTRANSv2b larval transport model (North et al., 2008, 2011; Schlag and North, 2012) that has recently been implemented in the J-SCOPE system and adapted for megalopae (Norton et al., *in revision*).

3. Results

3.1. Elemental and crystalline characterization of the carapace

The compilation of our results demonstrate that the carapace is highly mineralized and precipitated into a chitin-proteinaceous matrix. XRD identify calcite as a primary polymorph in the carapace. The mineralized exoskeleton of the megalopae intermolt stages consists of the thinner exocuticle on the surface that is $<2\text{--}3\ \mu\text{m}$ thick, and the thicker and more compact endocuticle underneath (Fig. 1) of approximately $6\text{--}7\ \mu\text{m}$, with the combined thickness up to $10\ \mu\text{m}$. The carapace surface is extensively covered with setae that are rooted in the calcified neuritic canals each with an average of about $5\ \mu\text{m}$ surface opening (Figs. S2 and S3). EDXS investigations characterized detailed elemental structure with average Ca^{2+} content of 28% in the carapace and pereopods, with much higher Ca^{2+} found within in the mid layer and the endocuticle (higher than 50%) compared to $<20\%$ found in the exocuticle (Fig. 1). The carapace endocuticle contains also a high concentration of Mg^{2+} with some areas of the carapace exceeding 5% content, categorizing it as a more soluble high-Mg calcite. In addition, the internal side contain high concentrations of phosphorus (up to 6%) and strontium (up to 2%) on the inner endocuticle (Fig. 1). The percentage of different dissolution features is similar between the carapace and the pereopods, however with much less variation in all elements between the carapace and pereopods (Fig. S1). This elemental composition indicates that other crystalline forms of carbonate could be precipitated into a chitin-proteinaceous matrix, such as an amorphous calcium carbonate (ACC) crystalline layer, but the methods used were not suitable for ACC detection. The strong presence of autofluorescence prevented more precise detection of any other crystalline forms, despite extensive use of Raman spectroscopy for this purpose. Nevertheless, such elemental structure resembles a layer of ACC with Mg^{2+} , phosphate and carbonate-rich phase, or ACC with magnesian calcite, as previously demonstrated in the edible crabs *Cancer pagurus* (Fabritius et al., 2012).

3.2. Megalopae habitat characterization with strong vertical and spatial Ω_{calc} vertical gradients

Crab megalopae were found in both outer-shelf, slope, as well as nearshore ($<200\ \text{m}$ depth) habitats, with distinctly different vertical

environmental gradients in the upper water column. Due to the upwelling of deeper, colder, CO₂-rich waters in the near-shore and coastal habitats, steep gradients in low pH and Ω_{cal} values were observed. In comparison, offshore region were characterized with more uniform vertical gradients with lower vertical difference were over the same depth interval (Fig. 2). Pronounced steep OA-related vertical habitats were observed in the upper 60 m of the water column, here represented as the difference between the surface and 60 m depth ($\Delta\Omega_{\text{cal},60}$ or ΔpH_{60}), which is within the lower range of megalopae diel vertical migration habitat. Among all tested depths, statistical models comparing biological responses (e.g. exoskeleton dissolution, body parameters, abundance) with environmental conditions had the strongest associations using the 60 m vertical depth integrated value (e.g., external dissolution on body parts vs. $\Delta\Omega_{\text{cal}}$ had the highest $R^2 = 0.821$ at 60 m). Hereafter, all environmental data are reported using the 60 m depth integrated values. Coastal conditions recorded near-saturation Ω_{cal} values down to 1.4, pH down to 7.48, and pCO₂ up to 910 μatm (Table S1; Fig. 2). There were no observations of $\Omega_{\text{cal}} < 1$ or hypoxia, with similar oxygen ranges observed in the onshore and offshore regions, while average temperature that was by about 1.3 °C warmer offshore. Food availability was an order of magnitude higher in the onshore regions compared to offshore, with the highest chl-a values recorded at 25 $\mu\text{g/L}$ (Fig. 2).

Multiple environmental parameters co-varied (Fig. 3a) as observed in the RDA plot at 60 m depth (Fig. 3b). The first two axes of the RDA explained approximately 90% of the variation among the biological and environmental parameters. The first RDA axis was characterized by a $\Delta\Omega_{\text{cal},60}$ vertical gradient and external dissolution, with both having negative loadings along the RDA1 axis. Carapace width was negatively correlated with $\Delta\Omega_{\text{cal},60}$, whereas external dissolution was positively correlated, suggesting that larger individuals had less dissolution and were associated with lower gradients in $\Delta\Omega_{\text{cal},60}$. While OA parameters (pCO₂, pH) were all correlated as indicated by alignment with the second RDA axis, the collinearity with temperature was not significant. We found less collinearity among the environmental parameters related to the 60 m vertical gradients, such as $\Delta\Omega_{\text{cal},60}$, ΔO_2 , and ΔT_{60} . Here, we focused on the mechanistic drivers that are explicitly involved in the external dissolution processes, we have examined $\Delta\Omega_{\text{cal},60}$ in how it relates to external dissolution. Similarly, internal dissolution was negatively correlated with pCO₂ along the second axis with slightly higher loading along the RDA1, and also slightly negatively related with increased temperature. The implications of this association and how they related to model output (Fig. 7) will be explained below.

3.3. Megalopae carapace dissolution and reduced width as responses to variable OA parameters across vertical scales

Dissolution assessment on the external surface of the exocuticle and internal surface of the endocuticle of the megalopa's carapace and pereopod exoskeleton, was conducted only after confirming that sample preservation did not impact dissolution patterns, i.e. samples preserved in ethanol vs. flash frozen did not exhibit any significant difference in their dissolution features. Using a novel categorization scheme to semi-quantify dissolution features, including ridging structures, dissolved areas around neuritic canals, and exposed calcite crystals (Figs. 4, S1 and S2; Table S2), the individuals demonstrated various extents of these features present on the external side of the carapace and the pereopod exoskeleton (Fig. S2 and S3). On the carapace, the front and outer surfaces were the most affected (Figs. 4 and S3). On the pereopod exoskeleton, the thoracic segments and chelae had the most severe dissolution, while the distant parts were less affected (Fig. S3). On all of the examined individuals with external dissolution, we also found evidence for internal endocuticle dissolution, which was, on average, approximately half that observed on the external exocuticle surface.

Average dissolution on the exocuticle showed the strongest linear dependence with $\Delta\Omega_{\text{cal},60}$ (Fig. 5; $R^2 = 0.866$, $p < .001$), demonstrating that the habitats with the steepest 60 m vertical gradients results in the

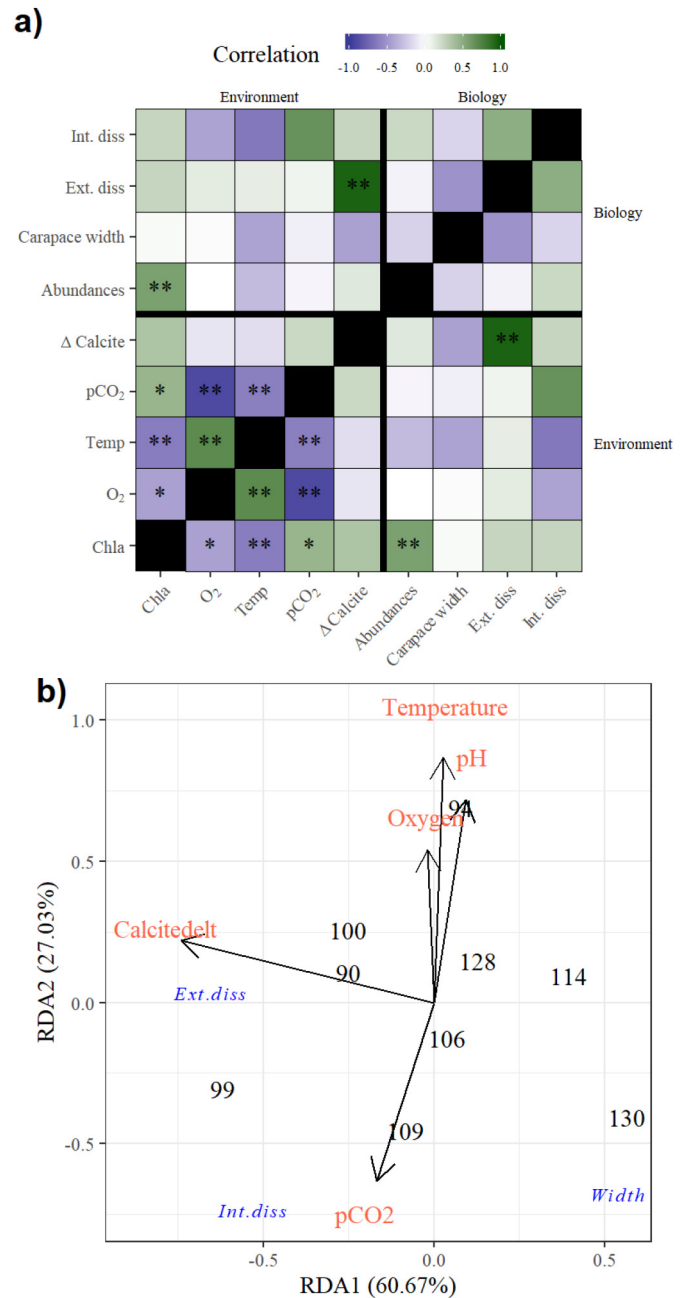


Fig. 3. Correlation matrix of environmental variables with biological endpoints for Dungeness megalopae: (a) Darker green values are strong positive correlations and darker purple values are strong negative correlations, while dimmer green and purple indicate weaker correlations; and (b) Redundancy analyses (RDAs) for environmental variables used in the analyses with crab biological measurements (internal and external dissolution, carapace width). (For interpretation of the references to colour in this figure legend, the reader is referred to the web version of this article.)

most damaged organisms. Because of the topographic features, there is a spatial variability related to the occurrence of the steepest $\Delta\Omega_{\text{cal},60}$ gradients, meaning that the lowest exoskeleton dissolution does not always correspond to the offshore gradients.

The internal dissolution showed the most robust evidence, though not statistically significant, of correlation with pCO₂ values (Fig. 5; $R^2 = 0.406$, $p = .065$) and negative marginal significance with temperature ($R^2 = 0.435$, $p = .053$). The internal dissolution rapidly intensified beyond pCO₂ > 500 μatm (Fig. 5b), with this being a robust threshold. There was no significant correlation between internal and external dissolution (Fig. 5; $p = .18$), suggesting decoupling of the two processes.

At sites with a small $\Delta\Omega_{\text{cal},60}$, the external surface of the carapace was characterized by predominantly smooth surfaces, the absence of dissolution, and the presence of setae (Figs. 7 and S2). Ridging features were present on all examined carapaces but significantly increased at the stations with the greatest $\Delta\Omega_{\text{cal},60}$ difference (Figs. 4 and 5). This presence of ridging features co-occurred with the increased occurrence of crystal exposure, ranging from increased porosity (Stage 1) to exposed crystals (Stage 2) at the sites with lower $\Delta\Omega_{\text{cal},60}$ difference, and deeper-protruding dissolution at the sites with greater $\Delta\Omega_{\text{cal},60}$ difference (Stage 2). Using image analysis, the depth of ridging structures was estimated at approximately 2 μm , around 25% of the cuticle thickness. Given the exocuticle thickness of 2–3 μm , the dissolution extended into the endocuticle (Fig. 6). The extent of dissolution on pereopod exoskeleton was comparable with the external dissolution, especially at the higher dissolution values (Fig. S5; $R^2 = 0.65$; $p = .0047$, slope = 0.901), indicating that both features were reliable metrics for dissolution assessment.

There was a distinct pattern of severe dissolution specifically developed around the calcified neuritic canals (Fig. 6). In megalopae collected at inshore stations (<200 m bottom depth), the carapace surface around the neuritic canals was markedly dissolved (Stage 2), and mechanoreceptors were often absent. Dissolution around the neuritic canals appeared to alter the morphology of the setae (Fig. 6). Setae edges were partially collapsed at the places where the mechanoreceptors are anchored in, with the initial ridging features around the canals degenerated into severely dissolved surfaces at the more intense $\Delta\Omega_{\text{cal},60}$ values (Fig. 6). On the megalopae from offshore stations with a smaller $\Delta\Omega_{\text{cal},60}$ the mechanoreceptors were present with no damage around the neuritic canals and less severe dissolution. Within the region of altered setae, dissolution up to 2–3 μm around the setae (Fig. S4) was accompanied by significant canal deformation. This deformation appears to destabilize the attachment of the setae anchor, resulting in the setae 'outrooting'. In some of the calcified neuritic canals, we noted the absence of setae but have not yet quantified the frequency of this occurrence.

To examine whether external or internal dissolution affects organismal or even potentially population-level metrics, dissolution measures were compared to megalopae body parameters and abundance. Here, we made an assumption that all the larvae were released at the same time to be able to compare different length parameters. We detected a significant negative correlation between external dissolution and width, as indicated by reduced individual carapace width (CW; $F = 18.61$, $R^2 = 0.823$, $p = .013$ for the regression of CW against external dissolution on body parts; $F = 5.3$, $R^2 = 0.57$, $p = .08$ for the regression of CW against all external dissolution; Fig. 5d), which is particularly strong in the coastal stations. This demonstrates that external OA-related exposure can indirectly result in reduced larval width. Carapace width was strongly oriented along the first RDA axis (Fig. 3), while being orthogonal to internal dissolution and directly opposed to external dissolution. The latter aligns with previous findings that internal dissolution is uncoupled from carapace width (linear model $p > .05$), whereas external dissolution is significantly associated with carapace width (RDA plot). Other length-related parameters (CL, R-DCS, TL) were not affected by OA parameters, demonstrating that only specific body parameters, *i.e.*, width are affected at more severe $\Delta\Omega_{\text{cal},60}$ vertical gradients.

On the higher, population-level response, only chl-a was found to be a significant driver. Abundance was positively correlated with chl-a at 60 m depth for both onshore and offshore habitats ($R^2 = 0.327$; $p = .008$). None of the other environmental parameters had a significant impact. However, in shallow coastal habitats with depth < 30 m, temperature was negatively related to larval abundance (for temperature at 10 m, $R^2 = 0.241$; $p = .02$; $F = 6.56$), although chl-a remained the dominant driver. In addition, neither carapace dissolution nor the width was related to larval abundance, suggesting decoupling of individual- and population-level effects of environmental conditions on larval Dungeness during the present day.

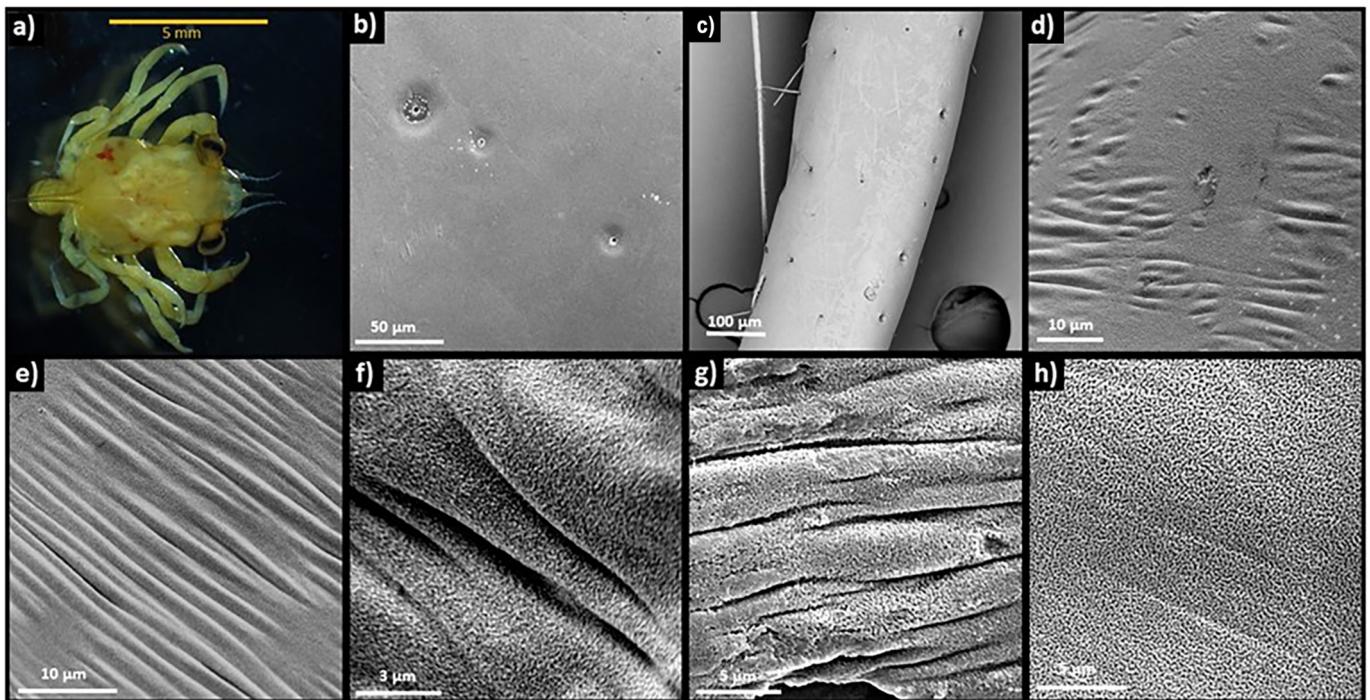


Fig. 4. External carapace and pereopod exoskeleton of the Dungeness crab megalopae (a) in its undamaged form (b, c) and with dissolution presence ranging from mild (Stage 1; d) to severe (Stage 2; e, f) patterns showing similarity in the structural damages (g) or exposed crystals (h). Indicated is the scale of the measurements (μm). The undamaged megalopae originated from the offshore or northwards habitats characterized by low $\Delta\Omega_{\text{cal},60}$ vertical gradients, while the most severely affected megalopae came from the nearshore or coastal habitats with steep $\Delta\Omega_{\text{cal},60}$ conditions. See more detailed explanation of the exoskeleton dissolution in the Supplementary Figs. S2, S3.

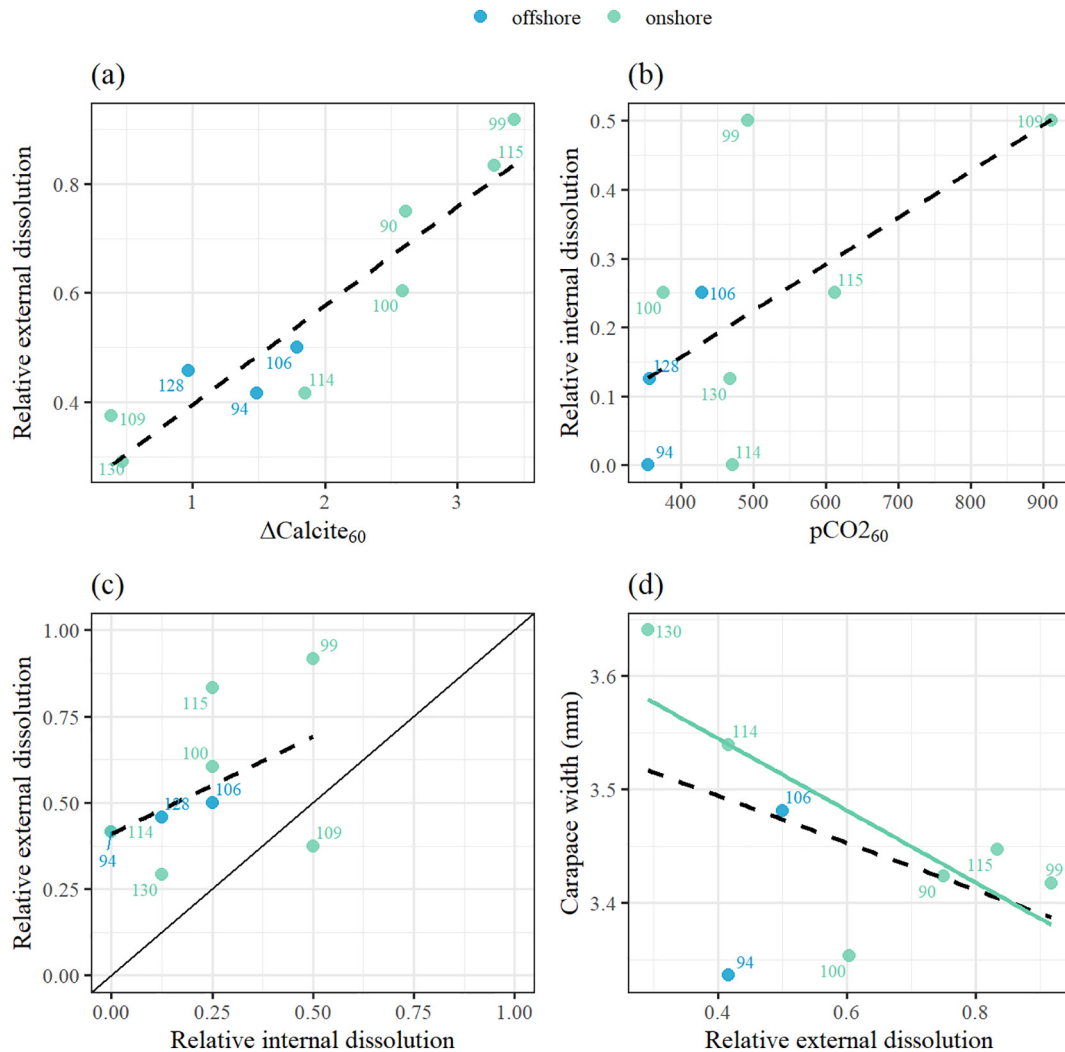


Fig. 5. Estimated linear relationships between ocean-acidification conditions and dissolution. Specifically for a) $\Delta\Omega_{\text{cal},60}$ and relative external dissolution ($R^2 = 0.87$; $p < .001$) with the equation of relative external dissolution = $0.181 \cdot \Delta\Omega_{\text{cal},60} + 0.215$; b) Depth-integrated $\text{pCO}_{2,60}$ and relative internal dissolution ($R^2 = 0.41$; $p = .064$); c) Comparison of the relative external and internal dissolution ($R^2 = 0.24$; $p = .18$); and d) Relative external dissolution and carapace width ($R^2 = 0.57$; $p = .08$). Dotted lines show the linear regression fit between all points. The solid line in (c) is the 1:1 line and the green line in (d) is the regression fit only through the onshore points. See methods for explanation of the term relative dissolution. Carapace width is in mm. (For interpretation of the references to colour in this figure legend, the reader is referred to the web version of this article.)

3.4. Megalopae exposure history to coastal OA conditions during the month prior to sampling

Particle back-tracking results with simulated vertical migration between the ocean surface and 60 m depth over a 30-d period from the J-SCOPE simulations showed that megalopae that were released in coastal habitats (<200 m), remained in coastal habitat for nearly a month of simulation regardless of their position in the domain (Fig. 7). This retention results in extended exposure to steeper coastal vertical gradients in OA conditions (Fig. 2), and consequently, more intense dissolution (Fig. 5).

4. Discussion

To our knowledge this is the first time that OA-related dissolution of calcite structures *in situ* has been demonstrated for crustaceans. Our results indicate that it is the exposure to both parameters, $\Delta\Omega_{\text{cal},60}$ (*i.e.* the difference in calcite saturation depth between the surface and 60 m depth) and pCO_2 , set up by as well as prolonged (<1 month) retention in the coastal waters that characterizes the suite of *in situ* parameters determining the larval crab vulnerability. This primarily demonstrates

that it is not just the mean state OA conditions, but also the vertical difference in the water column that can induce negative biological responses. Using a retrospective prediction from a regression model (Fig. 5a), we estimate an 8.3% increase in the extent of external carapace dissolution over the last two decades. This post-hoc estimate was based on a ΔpH changes of 0.02 unit per decade (Carter et al., 2018), comparing current average with the extent of dissolution predicted from our regression model based on the *in situ* observations (Fig. 5a with the equation in the figure content) by using the estimated pH conditions two decades prior. This is a reasonable estimate since $\Delta\Omega_{\text{cal},60}$ is highly correlated with $\Delta\Omega_{\text{pH},60}$ ($F = 204.3$, $R^2 = 0.96$, $p < .001$, Fig. S6).

What makes this OA-dependent dissolution of megalopae particularly relevant is that the crab samples originated in the supersaturated conditions with respect to calcite (the lowest $\Omega_{\text{calc}} = 1.41$). Since the dissolution reported in other calcifiers has been demonstrated above Ω_{ara} of 1.4–1.5 (Bednaršek and Ohman, 2015; Bednaršek et al., 2016), we conclude that exoskeleton dissolution is initiated at higher $\Delta\Omega_{\text{cal},60}$ than predicted based on thermodynamic principles alone. Furthermore, using exposure metrics based on the biogeochemical model output demonstrates that 1-month long exposure in coastal habitats with large $\Delta\Omega_{\text{cal},60}$ values can result in significantly more dissolution than predicted based on snap-shot observational data. In comparison with

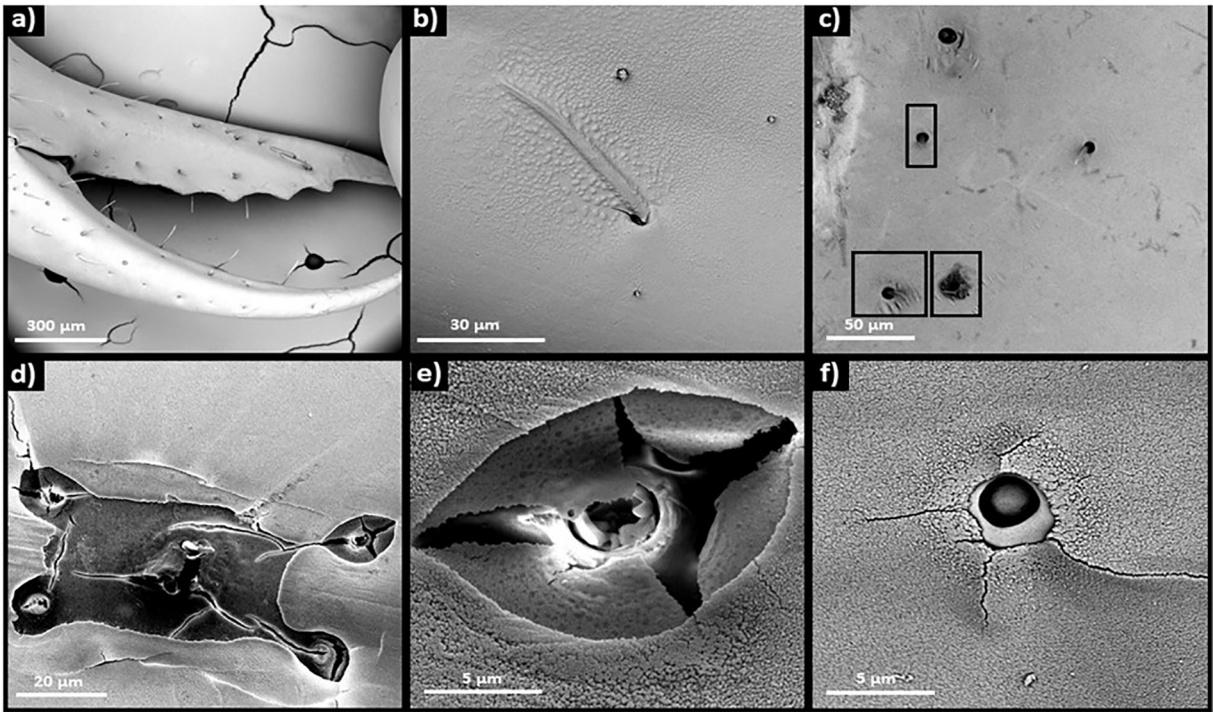


Fig. 6. Presence of setae on the pereopods (a) and carapace surface (b) of the megalopae on the intact individuals. The exposure to greater $\Delta\Omega_{\text{cal},60}$ differences mechanically damages the setae and results in their absence and outrooting (black squares) because of the dissolution around the neuritic canals (d, f) and damage with the collapsed structure (e).

the chemical observations, particle tracking model output indicates prolonged severity of exposure to the coastal low OA conditions, allowing for more extensive exoskeleton dissolution and reduced larval width in those habitats. It is worth noting that dissolution could be viewed as a physiological strategy to compensate against unfavorable external conditions. Dissolution of the outer calcite layer could increase the release of the bicarbonate and hydroxyl ions, raising pH, and providing a rapid alkalinization of the superficial layer (Kunkel et al., 2012). This alkaline layer could then provide an additional local protection from exposure to a large $\Delta\Omega_{\text{cal},60}$ conditions by blocking protons from continuously invading the internal fluid. However, as the larvae live in

highly dynamic environments, such a layer would be continuously disrupted, explaining the high extent of external dissolution.

4.1. Dissolution as a mechanism to offset OA-related extracellular acid-base disturbance?

Species with a developed capacity for ion exchange to maintain extracellular acid-base balance, are able to compensate for the effects of exposure to high $p\text{CO}_2$ waters and restore extracellular pH values optimal for physiological and biogeochemical processes (Somero, 1986). They do so via energetically expensive buffering of intra- and

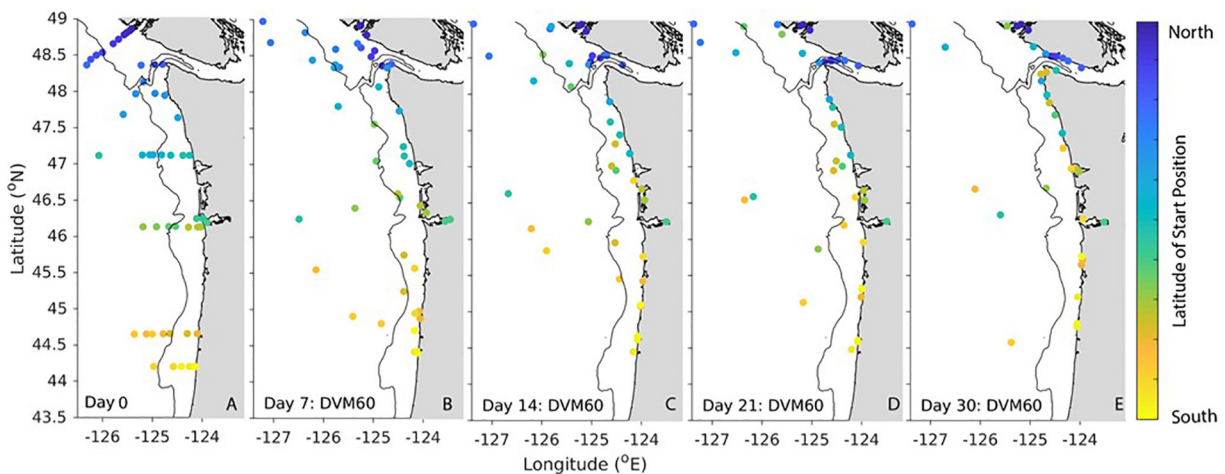


Fig. 7. Particle initialization locations (a) and average backtracked locations (b-e) for 7, 14, 21, and 30-day simulated particles exhibiting diel vertical migration (DVM) between 0 and 60 m depths. Replicate particles ($n = 100$) were initialized in the model at 51 locations representing the sampling stations for the 2016 West Coast Ocean Acidification Cruise. J-SCOPE's historical simulation of ocean conditions for 2016 was used to simulate advection of particles, and each particle exhibited vertical swimming between the ocean surface at night and a maximum daytime depth of 60 m. On a weekly basis, particle locations were averaged for all 100 particles initialized at the same station, which sometimes resulted in the average location being on land. These particles were moved to the nearest shoreline. Station colour varies by transect for improved resolution of dispersal patterns occurring at different latitudes. The 200 m isobath is shown for reference, and land is shaded in grey.

extracellular compartments achieved through various mechanisms, such as buffering by seawater-derived bicarbonate sources (Truchot, 1979), and increased respiratory activity to reduce CO₂ loading of the extracellular fluid and non-bicarbonate buffering (Cameron, 1985; Hans et al., 2014; Michaelidis et al., 2005).

However, the downside to the well-established extracellular acid-base control is an energetically demanding process (Hans et al., 2014; Michaelidis et al., 2005; Pane and Barry, 2007; Trigg et al., 2019). Therefore, we hypothesize that the internal carapace dissolution we observed in our study could be a part of a passive ability to buffer reductions in extracellular pH, a feature found in a variety of marine invertebrates including bivalves, echinoderms, and crustaceans (Cameron, 1985; Henry et al., 1981; Lindinger et al., 1984; Spicer and Taylor, 1987; Spicer et al., 2007). The narrow neuritic canals around the mechanoreceptors allow communication through secretion across the internal-external cuticle layers (Kunkel et al., 2012). While we currently have no information on the acid-base balance within these larval crabs under prolonged exposure to steep pCO₂ vertical gradients because no controlled experiments have been conducted, we propose future studies to examine if internal dissolution could provide some level of bicarbonate ions for buffering at comparatively low cost.

Alternative hypothesis for explaining internal dissolution might be based on the severity of external dissolution extending much deeper (Fig. S4) to initiate the endocuticle dissolution. Once the dissolution of the external carapace dissolution is initiated, the mineralogical-elemental structure of the mid- and endocuticle can allow for more rapid progression. The presence of high-Mg²⁺ content in the endocuticle can cause more rapid dissolution (Andersson et al., 2008), while comparatively lower Ca²⁺ content on the outward side presumably results in a weaker carapace (Chen et al., 2008). In addition, chitin-proteinaceous matrix, such as an amorphous crystalline layer might be present, which could importantly contribute to additional dissolution. Furthermore, while the internal solubility extent may be compensated by phosphorus, it can increase hardness, thereby preventing propagation of fractures, and Sr²⁺ because it can replace Ca²⁺ in the mineralization process (Dodd, 1964). In contrast, the observation of less internal dissolution on the endocuticle side compared to the external dissolution could be due to a difference in biomineral composition. For instance, intermixing calcite in the endocuticle with organic polymers would create a durable, protective covering, which may prevent the more soluble high-Mg calcite in the endocuticle from dissolving (Chen et al., 2008). However, we have no observations of dissolution penetration all the way from the external to the internal side, we thus propose an acid-base balance strategy to be more feasible explanation for the internal dissolution.

4.2. Potential detrimental effect associated with carapace dissolution

One of the most important findings of this study is the correlation between carapace dissolution and the reduction in larval width. This could, overtime, potentially impact population dynamics. We suggest that the dissolution-length linkage could be explained by two different hypotheses: first, pronounced dissolution under severe $\Delta\Omega_{\text{cal},60}$ vertical gradients results in dissolution rate outpacing calcification rate. In this mismatch of rates of two different processes, calcification rate cannot fully compensate for dissolution and results in overall smaller width ('the mismatch' hypothesis). Alternatively, there could be an energetic implication behind the dissolution-induced slowdown in width. In this form of the hypothesis, an organism expends additional energy to increase calcification to counteract dissolution, thus resulting in an energetic trade-off that potentially compromises organismal growth (the 'trade-off' hypothesis).

Furthermore, for early Dungeness crab life stages in the near-future, the prediction of more frequent and prolonged exposures to more severe $\Delta\Omega_{\text{cal},60}$ gradients (Turi et al., 2016) could have potentially deleterious consequences in terms of behavioral and sensory impairments and chelae function. First, dissolution-affected thinner structures may

become too weak to retain their integrity, particularly under more severe conditions and continuous water flow, resulting in ridged, puffed surfaces. Morphological changes may in turn negatively impact larval survival by altering swimming behaviors and competence, including the ability to regulate buoyancy, maintain vertical position, and avoid predators (Morgan, 1989; Sulkin, 1984). Similar morphological structures as those observed in our study were noted in the larval form of the European lobster (Agnalt et al., 2013), which under prolonged exposure to OA conditions led to irreparable carapace deformities, and these could lead to an increase in molt-related mortalities (Small et al., 2016). Second, dissolution on both sides of carapace and pereopod exoskeleton will inevitably limit the effectiveness of the exoskeleton in providing support for muscles contraction and defense from predators, aiding homeostatic functions, and enabling feeding functions. Third, calcified neuritic canals appear to be one of the dissolution hotspots compromising setae function. Compared with undamaged setae at undissolved surfaces (Figs. 6 and S2, S3), dissolved areas may not provide sufficient structural integrity for the setae (Fig. 6), potentially impairing their functionality. Given the role of setae as mechanoreceptors directly involved in supporting crustacean sensory and behavior processes, we hypothesize that the absence or damage of setae within their neuritic canals may in part provide a mechanistic understanding for potential aberrant behavioral patterns found across various crustacean species under low OA conditions, such as slower movement, less tactile recognition, and prolonged searching time, as well as impaired swimming (Alenius and Munguia, 2012; Dissanayake and Ishimatsu, 2011) and behavioral choice (de la Haye et al., 2011). These changes can result in impaired competitiveness and altered predator-prey relationships for crabs (de la Haye et al., 2012; Dodd et al., 2015; Landes and Zimmer, 2012; Wang et al., 2018). Fourth, it is currently unknown whether external dissolution in megalopae could carry over into later life stages, including the reproductively active adult stage, and what the potential consequences may be for the population dynamics. However, reduced calcification could result in poor mineralization through the intermolt period that would be especially devastating for larval crabs because of potentially smaller sizes at maturity, as well as increased vulnerability to predation during their most sensitive molting stage.

While OA parameters largely affect observed biomineralogical and organismal responses, population-level responses (*i.e.* abundances) are driven by food availability, with a lesser role for temperature in the near-shore conditions. Although biological responses at different levels of biological organization appear to be decoupled and responded to different drivers across temporal and spatial scales that need to be taken into account to improve biological forecasts and predictions. The only driver that seem to resonate across individual and population level, at least marginally, is the temperature, which might have an opposite effect on both levels. While warmer temperature negatively affects abundances, it also reduces internal dissolution, although the latter is only a marginally significant.

To more accurately predict large-scale vulnerability, it is important to consider population connectivity, related to essential population vital rates and affected by dispersal (Lowe and Allendorf, 2010). This can be partitioned into genetic connectivity and demographic connectivity, with our model outputs demonstrating onshore-offshore connectivity along the shelf-coastal and in the northern-southern directions. This implies prolonged exposure to less suitable habitats characterized by low $\Delta\Omega_{\text{cal},60}$ in the nearshore areas that can exacerbate negative biological effects but some of them could be counteracted by higher food availability. With respect to genetic connectivity, the status of Dungeness crab as a high gene-flow species with low genetic differentiation along the US West Coast and the lack of significant adaptation patterns (Jackson and O'Malley, 2017; Jackson et al., 2018; O'Malley et al., 2017) implies that the genetic pool that might allow for adaptation under future climate scenario will be limited. This points toward the need for more comprehensive population vulnerability assessment that can link OA vulnerability with the population genetics.

4.3. Future directions

Like dissolution in pteropods, larval dissolution observed in Dungeness crab is clear evidence that marine invertebrates are damaged by extended exposure to strong present-day OA-related vertical gradients in their natural environment. The unexplored aspect of OA impacts related to the damaged mechanoreceptors and potentially impaired sensory functions needs to be explored further. Namely, if the sensory functions are impaired, the transitioning from the larval to juvenile stage in their coastal habitat might be compromised under predicted scenarios of steeper ΔpH and $\Delta\Omega_{\text{cal},60}$ gradients (Gruber et al., 2012; Turi et al., 2016). Multiple pathways of larval vulnerability should be studied in the context of carry-over effects to the next juvenile benthic stage to explore whether crustacean molting can offset some of the detrimental effects. Such findings should be integrated into a population demographic and exposure history model that could eventually lead to improved management of Dungeness crab stocks (Fernandes et al., 2017; Lam et al., 2016).

Declaration of competing interest

The authors declare that they have no known competing financial interests or personal relationships that could have appeared to influence the work reported in this paper.

Acknowledgements

We thank Carry Weekes and Anna McLasky for collecting the larval individuals, Jennifer Fisher for providing guidance to Carry Weekes; Sten Littmann from Max Planck Institute in Bremen, Germany for elemental analyses. We are grateful to Polona Mrak and Miloš Vittori for analyses of the crab molting stages. We thank to Sandra Bigley for her editorial help with the manuscript.

Funding sources

This work was supported by the NOAA's Ocean Acidification Program for initial funding and NOAA Pacific Marine Environmental Laboratory (PMEL) for supporting NB, RAF, SRA, and SAS. This is PMEL contribution number 4906.

Appendix A. Supplementary data

Supplementary data to this article can be found online at <https://doi.org/10.1016/j.scitotenv.2020.136610>.

References

Agnalt, A.-L., Grefsrud, E.S., Farestveit, M., Larsen, M., Keulder, F., 2013. Deformities in larvae and juvenile European lobster (*Homarus gammarus*) exposed to lower pH at two different temperatures. *Biogeosciences* 10, 7883–7895.

Akaike, H., 1973. Information theory and an extension of the maximum likelihood principle. In: Petrov, B.N., Csaki, F. (Eds.), *Second International Symposium on Information Theory*. Akademiai Kiado, Budapest, Hungary, pp. 267–281.

Alenius, B., Munguia, P., 2012. Effects of pH variability on the intertidal isopod, *Paradella diana*. *Mar. Freshw. Behav. Physiol.* 45, 245–259.

Andersson, A.J., Mackenzie, F.T., Bates, N.R., 2008. Life on the margin: implications of ocean acidification on mg-calcite, high latitude and cold-water marine calcifiers. *Mar. Ecol. Prog. Ser.* 373, 265–273.

Bednaršek, N., Ohman, M.D., 2015. Changes in pteropod distributions and shell dissolution across a frontal system in the California current system. *Mar. Ecol. Prog. Ser.* 523, 93–103.

Bednaršek, N., Tarling, G.A., Bakker, D.C., Fielding, S., Cohen, A., Kuzirian, A., McCorkle, D., Lézé, B., Montagna, R., 2012. Description and quantification of pteropod shell dissolution: a sensitive bioindicator of ocean acidification. *Glob. Chang. Biol.* 18, 2378–2388.

Bednaršek, N., Feely, R.A., Reum, J.C.P., Peterson, B., Menkel, J., Alin, S.R., Hales, B., 2014. *Limacina helicina* shell dissolution as an indicator of declining habitat suitability owing to ocean acidification in the California current ecosystem. *Proc. R. Soc. B Biol. Sci.* 281, 20140123.

Bednaršek, N., Johnson, J., Feely, R.A., 2016. Comment on peck et al: vulnerability of pteropod (*Limacina helicina*) to ocean acidification: Shell dissolution occurs despite an

intact organic layer. *Deep-Sea Research Part II: Topical Studies in Oceanography* 127, 53–56.

Bednaršek, N., Feely, R.A., Tolimieri, N., Hermann, A.J., Siedlecki, S.A., Waldbusser, G.G., McElhany, P., Alin, S.R., Klinger, T., Moore-Maley, B., Pörtner, H.O., 2017. Exposure history determines pteropod vulnerability to ocean acidification along the US west coast. *Sci. Rep.* 7, 4526.

Busch, D.S., McElhany, P., 2016. Estimates of the direct effect of seawater pH on the survival rate of species groups in the California current ecosystem. *PLoS One* 11, e0160669.

Cameron, J.N., 1985. Compensation of hypercapnic acidosis in the aquatic blue crab, *Callinectes sapidus*: the predominance of external sea water over carapace carbonate as the proton sink. *J. Exp. Biol.* 114, 197–206.

Carter, H.A., Ceballos-Osuna, L., Miller, N.A., Stillman, J.H., 2013. Impact of ocean acidification on metabolism and energetics during early life stages of the intertidal porcelain crab *Petrolisthes cinctipes*. *J. Exp. Biol.* 216 (8), 1412–1422.

Carter, B.R., Feely, R.A., Williams, N.L., Dickson, A.G., Fong, M.B., Takeshita, Y., 2018. Updated methods for global locally interpolated estimation of alkalinity, pH, and nitrate. *Limnology and Oceanography Methods* 16 (2), 119–131.

Chavez, F., Pennington, J.T., Michisaki, R.P., Blum, M., Chavez, G.M., Friederich, J., Messié, M., 2017. Climate variability and change: response of a coastal ocean ecosystem. *Oceanography* 30, 128–145.

Chen, P.-Y., Lin, A.Y.-M., McKittrick, J., Meyers, M.A., 2008. Structure and mechanical properties of crab exoskeletons. *Acta Biomater.* 4, 587–596.

Davis, S., Sylvia, G., Yochum, N., Cusack, C., 2017. Oregon Dungeness Crab Fishery Bioeconomic Model: A Fishery Interactive Simulator Learning Tool. Version 5.7. Prepared by Coastal Oregon Marine Experiment Station, Oregon State University and the Research Group, LLC for the Oregon Dungeness Crab Commission.

de la Haye, K.L., Spicer, J.L., Widdicombe, S., Briffa, M., 2011. Reduced sea water pH disrupts resource assessment and decision making in the hermit crab *Pagurus bernhardus*. *Anim. Behav.* 82, 495–501.

de la Haye, K.L., Spicer, J.L., Widdicombe, S., Briffa, M., 2012. Reduced pH sea water disrupts chemo-responsive behaviour in an intertidal crustacean. *J. Exp. Mar. Biol. Ecol.* 412, 134–140.

Dissanayake, A., Ishimatsu, A., 2011. Synergistic effects of elevated CO₂ and temperature on the metabolic scope and activity in a shallow-water coastal decapod (*Metapenaeus joyneri*; Crustacea: Penaeidae). *ICES J. Mar. Sci.* 68, 1147–1154.

Dodd, J.R., 1964. Environmentally controlled variation in the shell structure of a pelecypod species. *J. Paleontol.* 38, 1065–1071.

Dodd, L.F., Grabowski, J.H., Piehler, M.F., Westfield, I., Ries, J.B., 2015. Ocean acidification impairs crab foraging behaviour. *Proc. R. Soc. B Biol. Sci.* 282, 20150333.

Fabritius, H.O., Karsten, E.S., Balasundaram, K., Hild, S., Huemer, K., Raabe, D., 2012. Correlation of structure, composition and local mechanical properties in the dorsal carapace of the edible crab *Cancer pagurus*. *Z. Krist.* 227 (11), 766–776.

Feely, R.A., Alin, S., Carter, B., Bednaršek, N., Hales, B., Chan, F., Juranek, L., 2016. Chemical and biological impacts of ocean acidification along the west coast of North America. *Estuar. Coast. Shelf Sci.* 183, 260–270.

Feely, R.A., Okazaki, R.R., Cai, W.-J., Bednaršek, N., Alin, S.R., Byrne, R.H., Fassbender, A., 2018. The combined effects of acidification and hypoxia on pH and aragonite saturation in the coastal waters of the California current ecosystem and the northern Gulf of Mexico. *Cont. Shelf Res.* 152, 50–60.

Fernandes, J.A., Papatathanasopoulou, E., Hattam, C., Queirós, A.M., Cheung, W.W., Yool, A., Artioli, Y., Pope, E.C., Flynn, K.J., Merino, G., Calosi, P., Beaumont, N., Austen, M.C., Widdicombe, S., Barange, M., 2017. Estimating the ecological, economic and social impacts of ocean acidification and warming on UK fisheries. *Fish. Fish.* 18, 389–411.

Fox, J., Weisberg, S., 2011. *An R Companion to Applied Regression*. SAGE Publications, USA.

Giltz, S.M., Taylor, C.M., 2017. Reduced growth and survival in the larval blue crab *Callinectes sapidus* under predicted ocean acidification. *J. Shellfish Res.* 36, 481–485.

González-Gordillo, J.I., Rodríguez, A., Queiroga, H., 2004. Characterization of the megalopal premoult stages of the green crab, *Carcinus Maenas* (Decapoda, Portunidae), from laboratory culture. *J. Crustac. Biol.* 24, 502–510.

Gravinese, P.M., Enochs, I.C., Manzello, D.P., van Woessik, R., 2018. Warming and pCO₂ effects on Florida stone crab larvae. *Estuar. Coast. Shelf Sci.* 204, 193–201.

Gruber, N., Hauri, C., Lachkar, Z., Loher, D., Frölicher, T.L., Plattner, G.-K., 2012. Rapid progression of ocean acidification in the California current system. *Science* 337, 220–223.

Hans, S., Fehsenfeld, S., Treberg, J.R., Weihrauch, D., 2014. Acid–base regulation in the Dungeness crab (*Metacarcinus magister*). *Mar. Biol.* 161, 1179–1193.

Henry, R.P., Kormanik, G.A., Smatresk, N.J., Cameron, J.N., 1981. The role of CaCO₃ dissolution as a source of HCO₃⁻ for the buffering of hypercapnic acidosis in aquatic and terrestrial decapod crustaceans. *J. Exp. Biol.* 94, 269–274.

Hobbs, R.C., Botsford, L.W., Thomas, A., 1992. Influence of hydrographic conditions and wind forcing on the distribution and abundance of Dungeness crab, *Cancer magister*, larvae. *Can. J. Fish. Aquat. Sci.* 49, 1379–1388.

Hodgson, E.E., Kaplan, I.C., Marshall, K.N., Leonard, J., Essington, T.E., Busch, D.S., Fulton, E.A., Harvey, C.J., Hermann, A.J., McElhany, P., 2018. Consequences of spatially variable ocean acidification in the California current: lower pH drives strongest declines in benthic species in southern regions while greatest economic impacts occur in northern regions. *Ecol. Model.* 383, 106–117.

Jackson, T.M., O'Malley, K.G., 2017. Comparing genetic connectivity among Dungeness crab (*Cancer magister*) inhabiting Puget Sound and coastal Washington. *Mar. Biol.* 164 (6), 123.

Jackson, T.M., Roegner, G.C., O'Malley, K.G., 2018. Evidence for interannual variation in genetic structure of Dungeness crab (*Cancer magister*) along the California current system. *Mol. Ecol.* 27 (2), 352–368.

- Kaplan, I.C., Williams, G.D., Bond, N.A., Hermann, A.J., Siedlecki, S.A., 2016. Cloudy with a chance of sardines: forecasting sardine distributions using regional climate models. *Fish. Oceanogr.* 25, 15–27.
- Kunkel, J.G., Nagel, W., Jercinovic, M.J., 2012. Mineral fine structure of the American lobster cuticle. *J. Shellfish Res.* 31, 515–526.
- Lam, V.W.Y., Cheung, W.W.L., Reygondeau, G., Sumaila, U.R., 2016. Projected change in global fisheries revenues under climate change. *Sci. Rep.* 6, 32607.
- Landes, A., Zimmer, M., 2012. Acidification and warming affect both a calcifying predator and prey, but not their interaction. *Mar. Ecol. Prog. Ser.* 450, 1–10.
- Lindinger, M.I., Lauren, D.J., McDonald, D.G., 1984. Acid-base balance in the sea mussel, *Mytilus edulis*. III. Effects of environmental hypercapnia on intra- and extracellular acid-base balance. *Marine Biology Letters* 5, 371–381.
- Long, W.C., Swiney, K.M., Foy, R.J., 2016. Effects of high pCO₂ on Tanner crab reproduction and early life history, part II: carryover effects on larvae from oogenesis and embryogenesis are stronger than direct effects. *ICES J. Mar. Sci.* 73 (3), 836–848.
- Lowe, W.H., Allendorf, F.W., 2010. What can genetics tell us about population connectivity? *Mol. Ecol.* 19, 3038–3051.
- Manno, C., Rumolo, P., Barra, M., d'Albergo, S., Basilone, G., Genovese, S., Mazzola, S., Bonanno, A., 2019. Condition of pteropod shells near a volcanic CO₂ vent region. *Mar. Environ. Res.* 143, 39–48.
- Melzner, F., Gutowska, M.A., Langenbuch, M., Dupont, S., Lucassen, M., Thorndyke, M.C., Bleich, M., Pörtner, H.O., 2009. Physiological basis for high CO₂ tolerance in marine ectothermic animals: pre-adaptation through lifestyle and ontogeny? *Biogeosciences* 6 (3), 4693–4738.
- Michaelidis, B., Ouzounis, C., Palaras, A., Pörtner, H., 2005. Effects of long-term moderate hypercapnia on acid-base balance and growth rate in marine mussels *Mytilus galloprovincialis*. *Mar. Ecol. Prog. Ser.* 293, 109–118.
- Miller, J.J., Maher, M., Bohaboy, E., Friedman, C.S., McElhany, P., 2016. Exposure to low pH reduces survival and delays development in early life stages of Dungeness crab (*Cancer magister*). *Mar. Biol.* 163, 118.
- Morgan, S.G., 1989. Adaptive significance of spination in estuarine crab Zoeae. *Ecology* 70, 464–482. <https://doi.org/10.2307/1937551>.
- North, E.W., Schlag, Z., Hood, R.R., Li, M., Zhong, L., Gross, T., Kennedy, V.S., 2008. Vertical swimming behavior influences the dispersal of simulated oyster larvae in a coupled particle-tracking and hydrodynamic model of Chesapeake Bay. *Mar. Ecol. Prog. Ser.* 359, 99–115.
- North, E.W., Adams, E.E., Schlag, Z., Sherwood, C.R., He, R., Hyun, K.H., Socolofsky, S.A., 2011. Simulating oil droplet dispersal from the Deepwater Horizon spill with a Lagrangian approach. In: Liu, Y., Macfadyen, A., Ji, Z., Weisberg, R.H. (Eds.), *Monitoring and Modeling the Deepwater Horizon Oil Spill: A Record Breaking Enterprise*. Geophysical Monograph Series. American Geophysical Union, USA, pp. 217–226.
- Norton, E., Siedlecki, S.A., Kaplan, I.C., Hermann, A.J., Fisher, J., Morgan, C., Officer, S., Saenger, C., Alin, S.A., Newton, J.A., Bednaršek, N., Feely, R.A., 2020. The importance of environmental exposure history in forecasting Dungeness crab megalopae occurrence using J-SCOPE, a high-resolution model for the US Pacific northwest. *Front. Mar. Sci.* (in revision).
- Oksanen, J., Blanchet, F.G., Friendly, M., Kindt, R., Legendre, P., McGlinn, D., Wagner, H., 2019. *Vegan: Community Ecology Package*. R Package Version 2.5–5. Available at: <https://CRAN.R-project.org/package=vegan>.
- O'Malley, K.G., Corbett, K., Beacham, T.D., Jacobson, D.P., Jackson, T.M., Roegner, G.C., 2017. Genetic connectivity of the Dungeness crab (*Cancer magister*) across oceanographic regimes. *J. Shellfish Res.* 36 (2), 453–465.
- Pacific States Marine Fisheries Commission, 2019. Species Report: Commercial Land Catch: Metric-Tons (Mt), Revenue, and Price-per-Pound (Price/Lbs). Pacific States Marine Fisheries Commission, Portland, OR Available at: <https://reports.psmfc.org/pacfin/?p=501:1:5808950816361::NO::>; Accessed date: 25 March 2019.
- Paganini, A.W., Miller, N.A., Stillman, J.H., 2014. Temperature and acidification variability reduce physiological performance in the intertidal zone porcelain crab *Petrolisthes cinctipes*. *J. Exp. Biol.* 217 (22), 3974–3980.
- Page, T.M., Worthington, S., Calosi, P., Stillman, J.H., 2016. Effects of elevated pCO₂ on crab survival and exoskeleton composition depend on shell function and species distribution: a comparative analysis of carapace and claw mineralogy across four porcelain crab species from different habitats. *ICES J. Mar. Sci.* 74 (4), 1021–1032.
- Pane, E., Barry, J., 2007. Extracellular acid-base regulation during short-term hypercapnia is effective in a shallow-water crab, but ineffective in a deep-sea crab. *Mar. Ecol. Prog. Ser.* 334, 1–9.
- R Core Team, 2019. *R: A Language and Environment for Statistical Computing*. R Foundation for Statistical Computing Available at: <https://www.R-project.org/>.
- Schiffer, M., Harms, L., Pörtner, H., Mark, F., Storch, D., 2014. Pre-hatching seawater pCO₂ affects development and survival of zoea stages of Arctic spider crab *Hyas araneus*. *Mar. Ecol. Prog. Ser.* 501, 127–139.
- Schlag, Z.R., North, E.W., 2012. Lagrangian TRANSport model (LTRANS v.2) User's Guide. University of Maryland Center for Environmental Science, Horn Point Laboratory, Cambridge, Maryland.
- Shanks, A.L., 1995. Mechanisms of cross-shelf dispersal of larval invertebrates and fish. In: McEdward, L.R. (Ed.), *Ecology of Marine Invertebrate Larvae*. CRC Press, USA, pp. 324–367.
- Siedlecki, S.A., Kaplan, I.C., Hermann, A.J., Nguyen, T.T., Bond, N.A., Newton, J.A., Williams, G.D., Peterson, W.T., Alin, S.R., Feely, R.A., 2016. Experiments with seasonal forecasts of ocean conditions for the northern region of the California current upwelling system. *Sci. Rep.* 6, 27203.
- Sinclair, M., 1988. *Marine Populations: An Essay on Population Regulation and Speciation*. Washington Sea Grant. University of Washington Press, Seattle, Washington.
- Small, D.P., Calosi, P., Boothroyd, D., Widdicombe, S., Spicer, J.I., 2015. Stage-specific changes in physiological and life-history responses to elevated temperature and pCO₂ during the larval development of the European lobster *Homarus gammarus* (L.). *Physiol. Biochem. Zool.* 88, 494–507.
- Small, D.P., Calosi, P., Boothroyd, D., Widdicombe, S., Spicer, J.I., 2016. The sensitivity of the early benthic juvenile stage of the European lobster *Homarus gammarus* (L.) to elevated pCO₂ and temperature. *Mar. Biol.* 163, 53.
- Somero, G.N., 1986. Protons, osmolytes, and fitness of internal milieu for protein function. *Am. J. Phys. Regul. Integr. Comp. Phys.* 251, R197–R213.
- Somero, G.N., Beers, J.M., Chan, F., Hill, T.M., Klinger, T., Litvin, S.Y., 2015. What changes in the carbonate system, oxygen, and temperature portend for the northeastern Pacific Ocean: a physiological perspective. *BioScience* 66, 14–26.
- Spicer, J.I., Raffo, A., 2007. Widdicombe, S., influence of CO₂-related seawater acidification on extracellular acid-base balance in the velvet swimming crab *Necora puber*. *Mar. Biol.* 151, 1117–1125.
- Spicer, J.I., Taylor, A.C., 1987. Carbon dioxide transport and acid-base regulation in the blood of the beach-hopper *Orchestia gammarellus* (Pallas) (Crustacea: Amphipoda). *Ophelia* 28, 49–61.
- Sulkin, S.D., 1984. Behavioral basis of depth regulation in the larvae of brachyuran crabs. *Mar. Ecol. Prog. Ser.* 15, 181–205.
- Trigg, S.A., McElhany, P., Maher, M., Perez, D., Busch, D.S., Nichols, K.M., 2019. Uncovering mechanisms of global ocean change effects on the Dungeness crab (*Cancer magister*) through metabolomics analysis. *BioRxiv* 574798 (1 August).
- Truchot, J.P., 1979. Mechanisms of the compensation of blood respiratory acid-base disturbances in the shore crab, *Carcinus maenas* (L.). *J. Exp. Zool.* 210, 407–416.
- Tunnicliffe, V., Davies, K.T., Butterfield, D.A., Embley, R.W., Rose, J.M., Chadwick Jr., W.W., 2009. Survival of mussels in extremely acidic waters on a submarine volcano. *Nat. Geosci.* 2, 344–348.
- Turi, G., Lachkar, Z., Gruber, N., Münnich, M., 2016. Climatic modulation of recent trends in ocean acidification in the California current system. *Environ. Res. Lett.* 11, 014007.
- Wang, Y., Hu, M., Wu, F., Storch, D., Pörtner, H.-O., 2018. Elevated pCO₂ affects feeding behavior and acute physiological response of the Brown crab *Cancer pagurus*. *Front. Physiol.* 9, 1164.